ISSN: 2472-3703 DOI: 10.6911/WSRJ.202304_9(4).0029

Effect of Hf doping on Structural, Surface Morphology, And Optical Properties of CdS: Hf Thin Films Deposited by RF Magnetron Sputtering

Wei Zou, Yong Cheng*, Qingyun Chen, Xinyu Li

College of Science, Guilin University of Technology, Guilin 541004, PR China

*Corresponding author: E-mail addresses: hb_cy@163.com

Abstract

This study focuses on the investigation of RF power variations (4-10W) effects on structural, morphological, and optical properties of CdS:Hf thin film deposited on Silicon/quartz substrate in a non-reactive atmosphere (Ar). The surface morphology, structure, optical and humidity sensing properties of the synthesized CdS:Hf thin films have been studied by X-ray diffraction (XRD), atomic force microscopy (AFM), field emission scanning electron microscopy (FESEM), energy-dispersive X-ray spectroscopy (EDX), X-ray photoelectron spectroscopy (XPS) and ultraviolet-visible spectrophotometry (UV-Vis). It was confirmed by XRD analysis that the thin films were produced are CdS:Hf with a hexagonal crystal structure. The CdS:Hf thin films present a polycrystalline, uniform, and porous structure. AFM shows that the increase of Hf doping has a significant change in the average roughness, root means square roughness, and the largest peak height of CdS:Hf films. XPS analysis of all films consisted mainly of Cd-S, Hf-S, and S-O chemical bonds. The experimentally measured optical band gap (E_g)ranges from 2.30 to 2.42 eV. Furthermore, the E_g value of CdS:Hf films decreases with the increase of Hf doping. The results show that the change of Hf doping is one of the important process parameters in RF magnetron sputtering, which will affect the morphology and optical properties of CdS:Hf films.

Keywords

CdS:Hf thin films; Optical properties; Magnetron sputtering RF; Optical energy bandgap.

1. INTRODUCTION

CdS thin films with high resistivity and optical transparency, good crystal symmetry, and higher thermal and chemical stability have been widely used in CdTe[1], Cu(In, Ga)Se_2[2], $BaSi_2$[3], Cu_2ZnSnS_4(CZTS)[4] based solar cells and window layer materials for photodetectors [5]. CdS is an n-type II–VI semiconductor with two crystal structures, cubic sphalerite, and hexagonal fiber zinc ore, with a direct band gap of 2.4 eV and an exciton binding energy of 28 MeV[6-9]. It has been widely used in optoelectronic materials due to its high optical transmittance in the visible spectral range between 400 and 800 nm[10-13]. CdS have excellent optical and electrical properties and are relatively simple to prepare, as well as good optical sensitivity; it has been widely studied and applied in the photocatalytic degradation of various organic pollutants[14-16]; for example, it is considered one of the most promising materials for window materials using its solar energy for hydrogen precipitation[17, 18].

The following methods for the preparation of CdS films have been reported: radio frequency (RF)[19], magnetron sputtering (PVD) [20], chemical bath deposition (CBD) [21],

ISSN: 2472-3703 DOI: 10.6911/WSRJ.202304_9(4).0029

electrodeposition (ED) [22], and vacuum evaporation[23] have all been practically applied. The above-mentioned techniques have been applied in practice. Different techniques, precursors, media, and temperatures are used to modify CdS films by the above-mentioned methods[24-26].

To enhance the photoelectric properties of CdS, different doping elements are usually added to the films to increase the carrier concentration. For example, Shakir et al.[27] successfully prepared Sm-doped CdS nanostructured films using the surface spray pyrolysis technique, and Sm doping in CdS films can improve the linear and nonlinear optical properties such as absorption spreading, energy band gap reduction, refractive index, and magnetization. Wang et al.[28] studied the effect of different Cu doping amounts on CdS films by using RF magnetron sputtering deposition of Cu-doped CdS films, and the results showed that Cu doping amounts had a greater increase in photoelectric density and current density. Ma et al.[29] used RF deposition of the CdS transition layer, followed by chemical bath deposition (CBD) of CdS nanofilms and annealed Cd/Si heterojunctions, and the results showed that the doping amount of Si could make the CdS/Si heterojunctions exhibit typical rectification characteristics. Chavez et al.[30] analyzed the effect of Al doping effect on heterojunctions by CBD deposition of Al-doped CdS thin films, and the results showed that The amount of Al doping was related to the electrical properties. Ashraf et al.[31] deposited Tb onto the Ag/Y:CdS/Ag film by magnetron sputtering deposition and the Tb doping amount has a faster response time compared to pure CdS devices. Shkir. et al.[32] prepared high-quality La@CdS films by spray pyrolysis and analyzed the optical switching behavior of the films, showing that the La doping has a significant increase in the optical intensity. Singh et al. [33] prepared Ag-doped n- CdS thin films by IGC technique and found that Ag doping significantly improved the recombination lifetime of carriers by comparing doped and undoped. Aboud et al. [34] used the spray pyrolysis technique for Cu-doped CdS thin films and showed that Cu doping significantly increased the activation energy in the optical band gap. Manthrammel et al. [35] studied the effect of Na doping on the deposition of CdS thin films by spray pyrolysis technique. The results showed that the amount of Na doping can significantly reduce the optical band gap. All of the above shows that the amount of metal doping can improve the optical properties.

Therefore, the selection of a suitable dopant is urgent, in the above method, magnetron sputtering is a convenient, low-cost, fast deposition process**.** First of all, so far, Hf has not studied the structural and optical properties of CdS films, and secondly, Hf has high stability, high transparency in the form of metal oxides, and wide application in the photovoltaic industry, so it has been selected as a doped element. Due to the inherent defects such as sulfur vacancies (V_S) and interstitial cadmium (I_{Cd}) atoms[36], CdS is doped by Hf to enhance the nonlinear optical parameters such as improve the optical properties, resistivity, and crystal structure. Studies have shown that Hf metal has good electrical conductivity, good oxidation resistance, thermal stability, thermal conductivity, and low electron escape is often used in plasma for plasma cutting motors projectors, magnetron sputtering targets, etc.[37] However, to date, no attempt has been made to study the influence of sputtering power on CdS:Hf films' basic properties such as their structural, surface morphological, and optical properties.

In this work, CdS:Hf films were prepared on Silicon substrate and quartz substrates by the co-sputtering method. By fixing the sputtering power of the CdS target and controlling the sputtering power of the Hf target, different Hf-doped CdS films can be obtained; the composition, microstructure, and systematic study of the optical properties of the prepared films were studied. The key to achieving better CdS:Hf film properties relies on a comprehensive understanding of the influence of sputtering power on its structural, physical, and optical properties.

ISSN: 2472-3703 DOI: 10.6911/WSRJ.202304_9(4).0029

2. EXPERIMENTS

2.1. Preparation of Hf-doped CdS films

Sintered cadmium sulfide targets and hafnium targets (60 mm diameter, 5 mm thickness, 99.99% purity) were used for the experiments. The Hf-doped cadmium sulfide films were prepared with a JGP-450a magnetron sputtering deposition system. High-purity argon (99.999%) was used as the working gas, and the background vacuum was 8×10^{-4} Pa. The Silicon substrate and quartz substrate were used so that the optical property of CdS:Hf thin films could be measured in the subsequent stage. CdS:Hf films with different Hf doping concentrations were prepared by using a CdS and Hf dual-target radio frequency (RF) magnetron co-sputtering method. The power of the CdS target was fixed, and the amount of Hf doping was adjusted by adjusting the power of the Hf target. The target surface was pre-sputtered for 3 min to remove possible contaminants. The substrates were cleaned with deionized water for 10 min, and then ultrasonically cleaned in acetone and anhydrous ethanol for 10 min. The power of the CdS target is 200W, the power of the Hf target is 4W, 6W, 8W, and 10W, the deposition pressure is 1.2Pa, and the prepared samples are CS1, CS2, CS3, and CS4. The details of RF magnetron sputtering parameters are tabulated in Table 1. The schematic image of the CdS:Hf film preparation process is illustrated in Figure 1.

2.2. Characterization

The CdS:Hf film surface was examined by a field emission scanning electron microscopy ((SEM, FEISirion200) linked with energy dispersive X-ray spectroscopy. The CdS:Hf film surface topography was imaged using an atomic force microscope (AFM) (Solver P47 AFM). The structures of the CdS:Hf films were examined by X-ray diffraction (GIXRD, Pert PRO the Netherlands, CuKa, λ=1.5406°). The energy spectrum structures of Cd, S, and Hf were tested by X-ray photoelectron spectroscopy (XPS, Thermo Fisher Scientific Company). The transmission and absorption spectra of the samples were obtained with a TU1, 800-visible spectrophotometer (TU1, 800UV-Visible).

Table 1. Experimental parameters of the deposition process in CdS:Hf thin films using an RF magnetron sputtering system

Deposition Parameters	Value
Operating pressure (mbar)	1.2
Base pressure (mbar)	8×10^{-4}
Ar flow ratio (sccm)	10
RF power of Hf target (W)	4,6,8,10
RF power of CdS target (W)	200
Target size (diameter × thickness) (mm)	60 × 5
Duration of deposition (min)	10
Deposition temperature	Ambient temperature
Substrate size (mm)	10 × 45 × 1

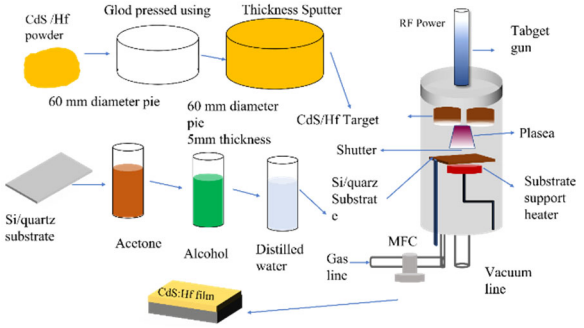

Figure 1. The schematic illustration of the fabrication of CdS:Hf film

ISSN: 2472-3703 DOI: 10.6911/WSRJ.202304_9(4).0029

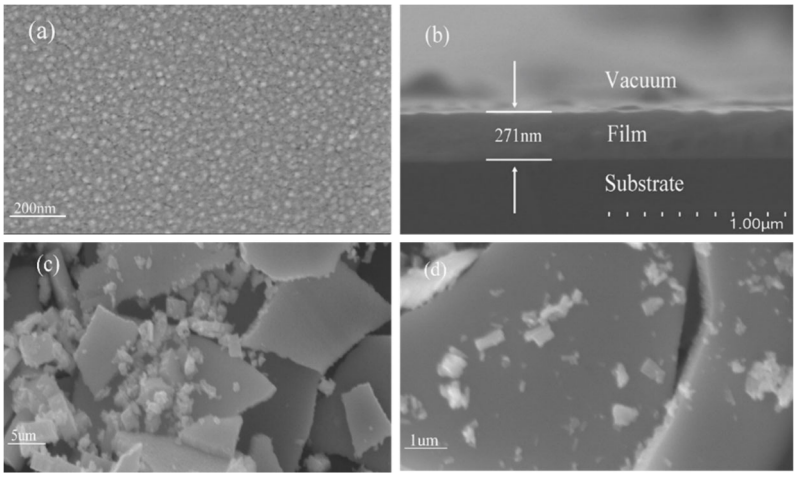

Figure 2. SEM image of CdS:Hf: (a),(c), and (d) surface and (b) cross-section.

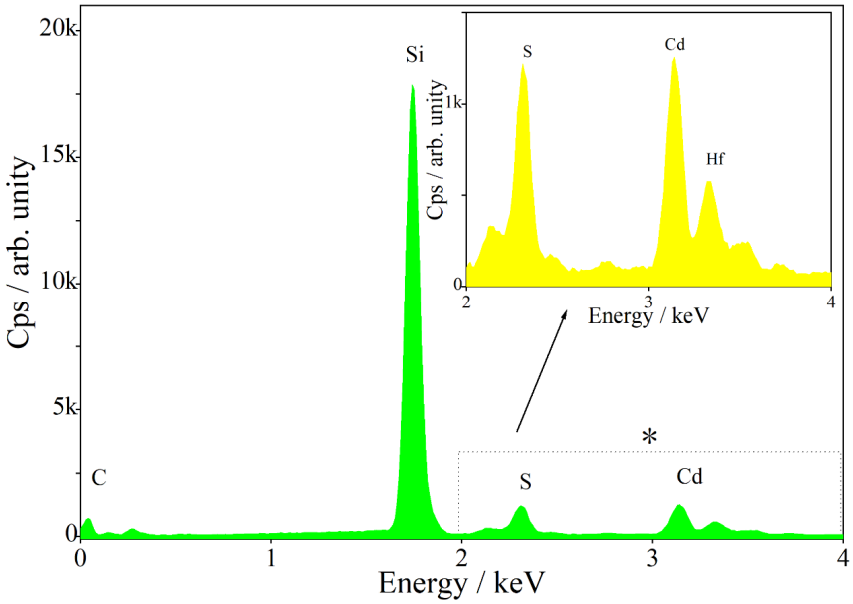

Figure 3. EDX spectrum of the CdS:Hf.

3. RESULTS AND DISCUSSION

3.1. SEM analysis of samples

The surface and cross-sectional morphology of CdS:Hf of sample CS4 are shown in Figure 2. CdS:Hf's surface is uniform and smooth and flat without cracks. Fig.2. a, c, and d show that the films prepared by magnetron sputtering are composed of ellipsoidal and polygonal nanoparticles with a size of about 10-20 nm, and no obvious voids or cavities are observed between the particle boundaries of all films. Fig.2b shows the morphology of the corresponding cross-section of the CdS:Hf films with a film thickness of 271 nm. The thicknesses of samples CS1, CS2, and CS3 were 265 nm, 269 nm, and 270 nm, respectively, indicating that the film thicknesses did not vary much. The CdS:Hf films were prepared in a pure Ar environment, all the film samples contain Cd, S, and Hf elements. the distribution of CdS:Hf film elements is shown in Figure 3.

3.2. AFM analysis of samples

The microscopic morphology of the CdS:Hf films were tested by atomic force microscopy (AFM), and the average roughness (RA), root mean square roughness (RMS), and the largest peak height (LPH) were analyzed. The variation in surface morphology and roughness can be

ISSN: 2472-3703 DOI: 10.6911/WSRJ.202304_9(4).0029

observed in the image in Figure 4 (3D). In Figure 4 (2D) it can be observed that the surface of the CdS:Hf film is columnar growth and the film surface is relatively homogeneous; it is continuous and dense with no pinholes or cracks between the grains. The film has no holes and the grains are uniformly distributed in size. RMS is defined as the average root mean square of the deviation from the height of the mean elevation plane, calculated from the relative height of each pixel in the image[38]:

$$R_{RMS}=\sqrt{\left(\frac{Z_1^2+Z_2^2+\cdots+Z_N^2}{N}\right)} \quad (1)$$

N denotes the number of points in the scanned area and Z is the average of all points.

Table 2 shows the LPH, AR, and RMS of samples deposited under different Ar partial pressures. As the amount of Hf doped increases, LPH, AR, and RMS are all gradually rising Sputtered high-energy particles are deposited on the substrate to form a thin film. AR from 3.155nm increased to 8.354nm (2D), RMS from 4 .086nm increased to 12 .079 nm (2D), and LPH from 3 to 2.467 nm increased to 56 445nm. AFM analysis showed that all CdS:Hf film samples were homogeneous, with well-defined nanoparticles Particles, the surface roughness is relatively small; the maximum peak height of sample CS1 is 32.467 nm, and sample CS4 surface maximum peak height of 56.445nm. With the increase of Hf target sputtering power, the AR of the film was 3.155nm, 6.092nm, 7.118nm, and 8.345nm, and the RMS of the thin film was 4.086nm, 8.570nm, 12.079 and 11.081nm, and the LPH of the thin film was 32.467nm, 34.339nm, 41.079nm, and 56.445nm, respectively. This is because the Concentration of Ar is higher at low hafnium doping levels, while Ar only bombards the surface of the film; anti-sputtering Some weak bonds in the film can be removed, so that the film is tightly bound and the particles are relatively small. This has led to an increase in LPH, AR, and RMS of the film, at the same time. The voids in the film are reduced, making the film more dense and uniform.

Table 2 LPH, AR, and RSM roughness of the CdS:Hf thin films

Power (W)	LPH(nm)	AR (nm)	RMS (nm)
4	32.467	3.155	4.086
6	34.339	6.092	8.570
8	41.079	7.118	11.081
10	56.445	8.345	12.079

Table 3 Interplanar spacing, lattice constant, grain size, chemical composition, and FWHM of CdS:Hf films deposited at different powers: a, c, and L

Power(W)	FWHM(deg.)	L(nm)	a(nm)	c(nm)	Chemical composition (at.%)			
					Cd	S	Hf	O
4	0.665	41	0.561	0.678	40.2	42.3	1.538	6.8
6	0.661	39	0.561	0.678	38.4	39.31	1.639	6.36
8	0.550	38	0.561	0.678	36.1	37.39	1.855	6.16
10	0.453	37	0.561	0.678	33.8	34.9	1.871	6.96

ISSN: 2472-3703 DOI: 10.6911/WSRJ.202304_9(4).0029

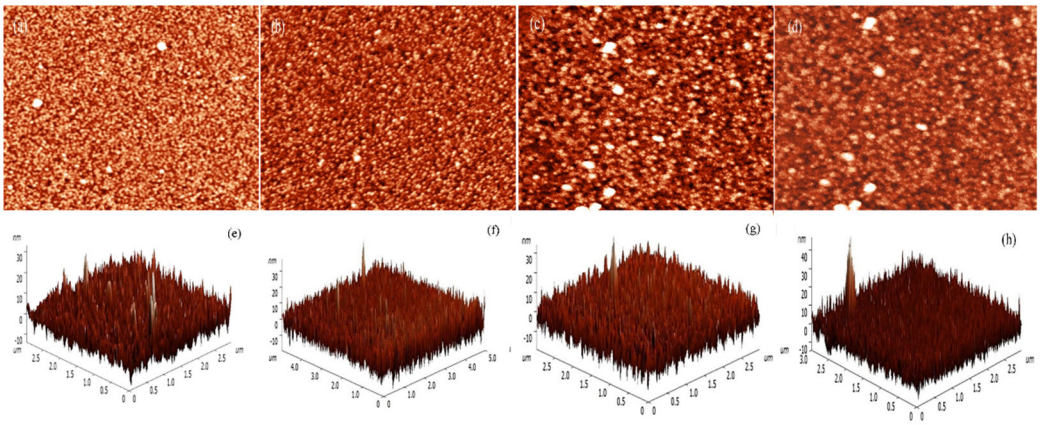

Figure 4. The surface AFM images of CdS:Hf thin films 2D (a,b,c,d) and 3D (e,f,g,h) with sputtering power of 4W, 6W,8W, and 10W, respectively

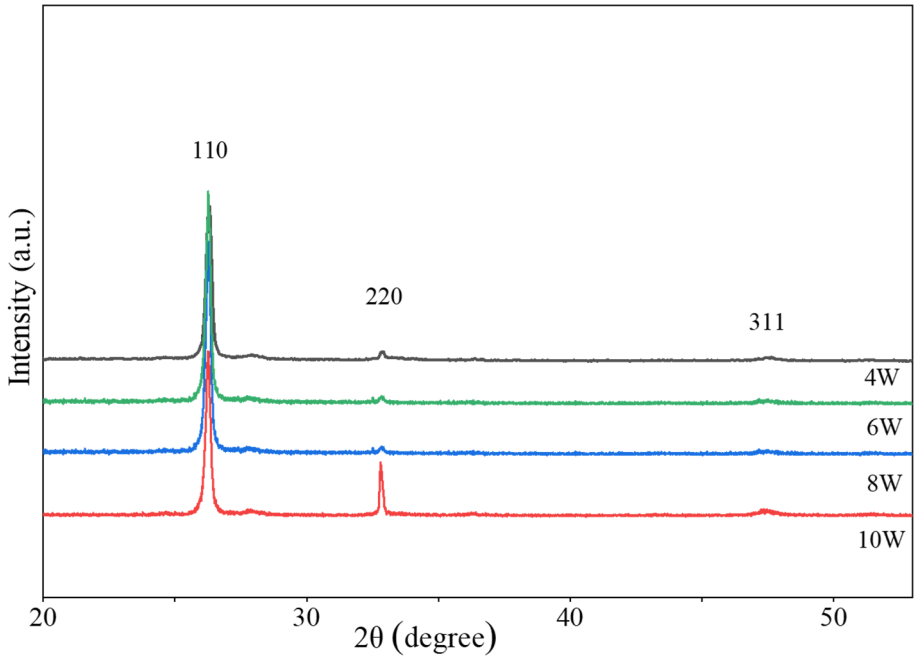

Figure 5. XRD pattern of CdS:Hf films

3.3. XRD analysis of samples

Figure 5 shows the XRD patterns of the CdS:Hf films, from which it can be seen that the peaks at 26.3°, 32.7°, and 47.5°correspond to the diffraction peaks in the crystallographic directions (110), (220), and (311), respectively. Among these peaks, the (110) peak is the strongest in the film, which confirms that this crystalline plane has the smallest surface energy to make the crystal grow in this direction, and the 2θ=26.3° diffraction peak corresponds to the hexagonal structure of cadmium sulfide since in thermodynamics the hexagonal structure is more stable than the cubic structure.[39] However, it can be observed that the peaks at 2θ=26.2° and 32.7° correspond to the hexagonal structure of cadmium sulfide in the (111), (220) planes. The diffraction crystal plane intensity of the main peak is due to the grain size and the amount of Hf doping leads to a change in the lattice parameters of CdS. A weaker peak at 2θ=47.5° is observed corresponding to the diffraction peak of Hf. The hexagonal spacing (a) and lattice constant (c) of the CdS:Hf films are 0.561 nm and 0.678 nm, respectively.

The structures of the thin film crystals were analyzed by XRD and compared with the data reported by JCPDS. The lattice constants, grain size, microstrain, crystalline phase, and

ISSN: 2472-3703 DOI: 10.6911/WSRJ.202304_9(4).0029

dislocation density of the films were calculated from the XRD spectra. From the XRD data, it can be seen that the interlayer spacing (d) is determined by Bragg'slaw[40]

$$n\lambda=2d\sin\theta \tag{2}$$

where n, λ, and θ are the order diffraction, X-ray wavelength, and diffraction angle, respectively The average grain size (L) of the prepared films was calculated using the Debye-Scherer relationship as follows[41]

$$L=\frac{K\lambda}{B\cos\theta} \tag{3}$$

where K and B are the constants (0.9) and full width at half maxima (FWHM), respectively

where (h, k, l) is the Miller index. In addition, the hexagonal interplanar spacing (a) and lattice constant (c) of the CdS films were determined by[42]

$$\frac{1}{d^2}=\frac{4}{3}\times\left(\frac{h^2+hk+l^2}{a^2}\right)+\frac{l^2}{c^2} \tag{4}$$

A comparative study of the diffraction peaks of all samples showed a gradual increase in the intensity of the diffraction peaks with increasing Hf doping concentration and a slight increase in the face spacing (d-spacing) values, which shifted the XRD peaks to the lower angular side. This is because the ionic radius of the doped element Hf is higher than that of Cd^{2+} located in the substitution sites of the cadmium sulfide lattice. A weaker diffraction peak associated with the metallic Hf or HfS_2 phase was observed at 2θ = 47.5° in the XRD analysis due to the very low number of dopant atoms or the substitution of Cd^{2+} ions by Hf^{4+} ions in the crystal, which inhibits the formation of CdS. Table 3 shows the grain size (L) and FWHM of the samples deposited at different Ar partial pressures. It can be seen that FWHM decreases with the increase of Hf content, indicating that the grain size decreases significantly with the increase of concentration; the grain size decreases from the initial 41.500 nm to 36.891 nm, and the amount of Hf doping can reduce the grain size of cadmium sulfide films. The decrease in grain size value of CdS:Hf films is because Hf^{4+} ions occupy the gap position in the lattice, resulting in an incomplete chemical reaction between the host ion and the doped ion. The increase in grain size is due to the ion radius of the dopant Hf^{4+} (2.16Å) being greater than the ion radius of Cd^{2+} (0.95Å). [43] Thus, as Hf^{4+} increases, the lattice expands, resulting in a larger crystal size; the grain size decreases because Hf^{4+} occupies both the substitution site and the gap site of the host lattice.

3.4. XPS analysis of samples

To analyze the changes in chemical composition, valence, and energy band structure of CdS: Hf films, the film composition was studied by XPS and AES. There are four distinct peak positions in the XPS spectrum of CdS:Hf films, corresponding to Cd 3d, S 2p, and Hf 4f; from the spectrograms, it can be seen that Cd, S, Hf, and O elements are present in the films, and a Gaussian fit of Cd 3d, S 2p, Hf 4f, and O 1s for the fitted spectrograms and calibrated using C 1s. The elemental composition of the films can be obtained from the XPS surface scans. It can be seen from the plot that the content of Hf in the film increases with increasing CS, while the content of Cd and S gradually decreases, as shown in Fig. 6. The stoichiometry of the film can be calculated from Figure 6. The stoichiometry values corresponding to samples CS1, CS2, CS3, and CS4 are $CdS_{1.11}Hf_{0.01}O_{0.65}$, $CdS_{1.39}Hf_{0.03}O_{0.61}$, $CdS_{1.68}Hf_{0.05}O_{0.66}$, and $CdS_{1.95}Hf_{0.08}O_{0.69}$, respectively.

ISSN: 2472-3703 DOI: 10.6911/WSRJ.202304_9(4).0029

Figure 7. shows the high-resolution peaks of S 2p at different CS. Three peaks corresponding to S-Cd, S-O, and S-Hf bonds were obtained by fitting with Gaussians. S-Hf bonds at 162.11 eV are present at different binding energies; peaks at about 161.60 eV can be distributed to S-Cd; peaks above 162.55 eV can be assigned to S-O bonding. Several factors cause the peak to move toward larger binding energies, namely surface contamination, and instrument sensitivity. As the doping amount of Hf increases, more S and Hf combine to form S-Hf bonds, so the content of S-Hf bonds gradually increases and the content of S-Cd bonds decreases due to more Hf replacing Cd to form S-Hf bonds. The above results indicate that S atoms are S-Hf and S-Cd bonded, respectively.

Figure 8. shows the Cd 3d spectra of different samples of CS and their peak fits, the peaks located at 405.20 eV and 412.05 eV correspond to Cd $3d_{5/2}$ and Cd $3d_{3/2}$, respectively, indicating that Cd is in the Cd^{2+} state. The peak Cd-S bond of Cd, but the content of the fitted Cd-S gradually decreases; the peak of Cd-S moves toward lower binding energies, confirming the presence of metallic Cd atoms, which is due to the amount of Hf doping leading to Cd^{2+} reduction of Cd monomers[39].

Figure 9. shows the Hf 4f spectra and peak fits for different samples of CS, with the peak at 18.40 eV for the Hf-S bond and 17.00 eV for the Hf-O bond. Meanwhile, the Hf-S bond increases gradually with the increase of Hf doping. It indicates that the Hf doping process formed chemical bonds with S.

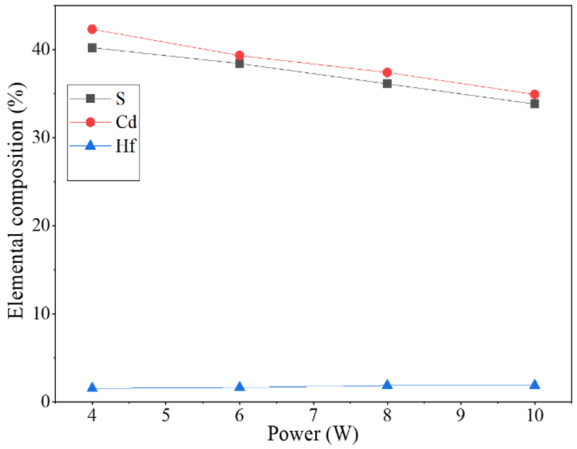

Figure 6. The composition of the elements S, Cd, and Hf in the film

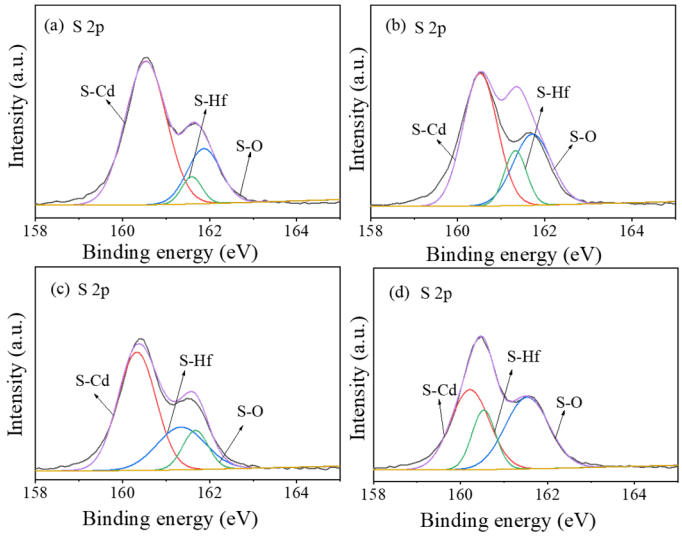

Figure 7. The S 2p spectrogram of different CS: (a) CS1; (b) CS2; (c) CS3; (d) CS4 and its peak fitting

ISSN: 2472-3703 DOI: 10.6911/WSRJ.202304_9(4).0029

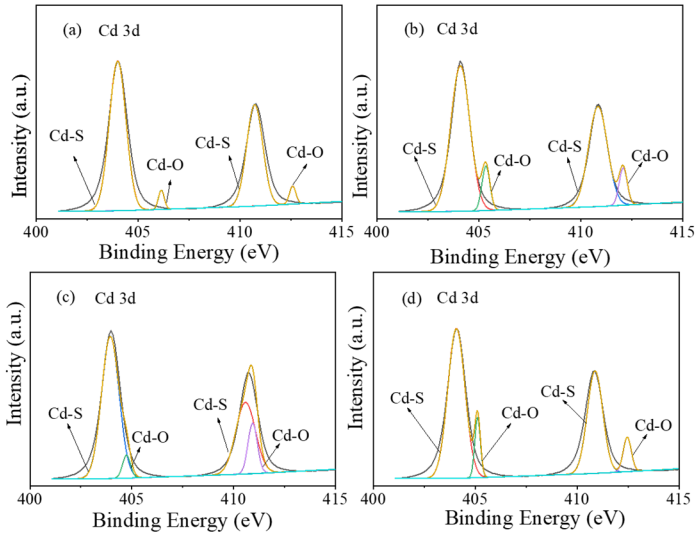

Figure 8. The Cd 3d spectrogram of different CS: (a) CS1; (b) CS2; (c) CS3; (d) CS4 and its peak fitting

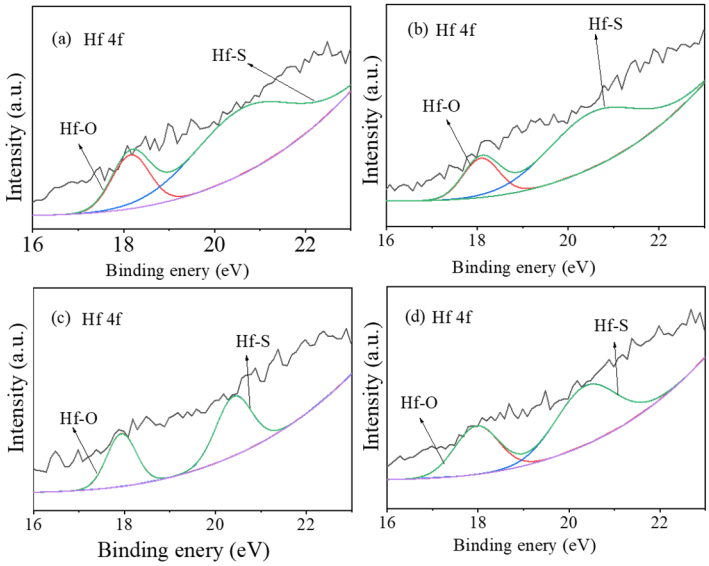

Figure 9. The Hf 4f spectrogram of different CS: (a) CS1; (b) CS2; (c) CS3; (d) CS4 and its peak fitting

3.5. Optical properties

Figure 10. shows the transmittance and optical band gap of CdS:Hf films prepared at different power levels. Figure 10 shows the UV-visible transmission spectrum of CdS:Hf films prepared with different amounts of Hf doped, with good transmittance in the infrared region. After different amounts of Hf doping, the transmittance of different CdS:Hf films is greatly improved. The CdS:Hf transmittance data improved significantly across the spectrum, showing that a more transparent CdS:Hf film sample was formed, and it was proved that Hf doping could significantly improve the light transmittance of The CdS film. The increase in CdS:Hf film transmittance is due to increased phonon scattering of doped crystal defects. In addition, the grain size of the crystal also plays an important role in determining the transmittance of the film; the increase in grain size also improves the light transmittance (T); the improvement of the transmittance is related to the crystalline properties of the film, which corresponds to the XRD diagram above. The blue shift of the transmission spectrum of the doping amount is explained by the sp-d orbital exchange interaction between local electrons with electrons and cationic position transition metals[44].

ISSN: 2472-3703 DOI: 10.6911/WSRJ.202304_9(4).0029

According to the transmission spectral profile of the film and the law of optical constants (1), the absorption coefficient of the film can be calculated

$$a = \frac{1}{d} In\left(\frac{100}{T}\right) \tag{5}$$

where T denotes the transmittance and d denotes the thickness of the film. Using the Tauc[45]equation (2), the optical bandgap of the film can be calculated

$$(ahv)^2 = A\left(hv - E_g\right) \tag{6}$$

where α, hv, and A denote the absorption coefficient, photon energy, and constant, respectively. From the relational curve of hv, the optical band gap was calculated by extrapolation. Figure 10 (b) shows that the optical band gaps of CdS:Hf films prepared at different doping amounts of Hf are 2.42 eV, 2.38 eV, 2.35 eV, and 2.30 eV, respectively. compared with the theoretical value in the literature (2.42eV), the optical band gaps of films prepared at different doping amounts of Hf are reduced by 0.12eV optical band gap in cadmium sulfide due to the smaller radius of S^{2-} than Cd^{2+}, which easily forms V_S, causing the formation of shallow or deep traps in the valence band of excited electrons. This is due to the presence of impurities in the conduction band (CB), and the appearance of many bulk effects in the CB and valence band (VB) that originate from impurity scattering and electron interactions[46]. The reduction in the optical bandgap is due to the quantum confinement of carriers; and also results in more electrons that can be excited by energy excitation, which promotes the separation of electrons and holes and increases the loading. This may be because after the hafnium is oxidized to produce hafnium dioxide, the hafnium atom radius is larger than the cadmium atom and can replace the cadmium vacancy V_{Cd} in the CdS lattice as a donor, thus providing carriers to reduce the optical bandgap. Therefore, as the Hf target power increases, leading to a significant increase in the free carriers occupying the bottom of the passband, the optical bandgap of the CdS:Hf film decreases.

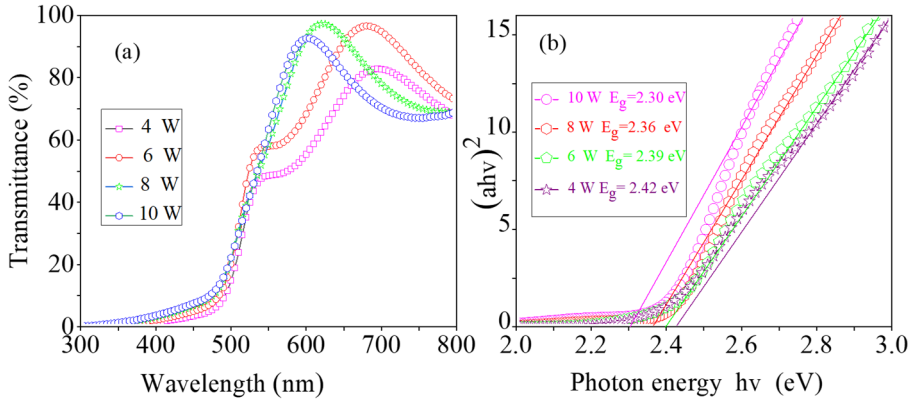

Figure 10. (a)Transmission spectrum of the CdS:Hf films (b) Relationship between $(\alpha hv)^2$and hv of the CdS:Hf film

4. CONCLUSION

CdS:Hf thin films were successfully deposited on the Silicon substrate and quartz substrate by RF magnetron sputtering. Effect of RF power (4-10) of Hf target on structure, morphology, and optical properties of CdS:Hf film. SEM images show that all of our sample surfaces are relatively smooth and uniform. XPS showed all thin film samples are mainly made of Cd -S, Hf-S, Cd-O, and S-O chemical bond composition. RA, RMS, and LPH were analyzed by AFM. AR

ISSN: 2472-3703 DOI: 10.6911/WSRJ.202304_9(4).0029

increased from 5.199 nm, RMS increased by 7.993 nm, and LPH increased by 23.978 nm. The structure of the thin film was analyzed by XRD, and the grain size was reduced by 4.601 nm. The transmittance and optical band gap of CdS:Hf films were analyzed by UV-Vis spectrophotometry and the optical bandgap is reduced by 0.12 eV. The research in this paper can provide new application prospects for the development of CdS:Hf films based on high-performance, adjustable frequency band selective photodetectors, and provide a reference for the application of CdS:Hf films in semiconductor optoelectronics and solar cells.

ACKNOWLEDGMENTS

The authors are grateful to the Doctoral Research Startup Program of the Guilin University of Technology (GLUTQD2006043).

REFERENCES

[1] M.K.A. Mohammed, Studying the structural, morphological, optical, and electrical properties of CdS/PbS thin films for photovoltaic applications, Plasmonics 15(6) (2020) 1989-1996.

[2] M.M.A.R. Moon, Md Ferdous Hossain, Jaker Ismail, Abu Bakar Md, Comparative study of the second generation a-Si:H, CdTe, and CIGS thin-film solar cells, Advanced Materials Research 1154 (2019) 102-111.

[3] M.M.A.R. Moon, Md Ferdous Kuddus, Abdul Hossain, Jaker Ismail, Abu Bakar Md, Investigation of thin-film p-BaSi2/n-CdS heterostructure towards semiconducting silicide based high efficiency solar cell, Physica Scripta 95(3) (2020) 035506.

[4] L.J. Liu, YuxiaoGao, Chao Xu, HejuZhao, Wei Dai, Weijie Yu, Wei Li, Xiaowei, Improving the performance of Cu2Zn(SnyGe1-y)(SxSe1-x)4 solar cells by CdS:Zn buffer layers, Journal of Alloys and Compounds 738 (2018) 158-163.

[5] A.K. Kumar, V. Chandra, R.Gautam, Y. K., Effect of sputtering process parameters on structural and optical properties of CdS thin films, Materials Research Express 6(10) (2019) 106448.

[6] A.S.M. Baron, K. A. Abood, M. M., The role of Ag layer in the optical properties of CdS thin film, Chalcogenide Letters 18(10) (2021) 585-588.

[7] S.L. Wang, X. Zhang, J.Y. Bie, H.P. Gong, M. Cao, S. Zhang, Y.C. Jiang, Y. Shen, L.J. Wang, Influence of Cu doping on physical and photo-electrochemical properties of CdS thin films prepared by RF magnetron sputtering, Materials Science in Semiconductor Processing 133 (2021) 105933.

[8] M. Shkir, I.M. Ashraf, A. Khan, M.T. Khan, A.M. El-Toni, S. AlFaify, A facile spray pyrolysis fabrication of Sm:CdS thin films for high-performance photodetector applications, Sensors and Actuators a-Physical 306 (2020) 111952.

[9] M.T. Khan, M. Shkir, B. Alhouri, A. Almohammedi, Y.A.M. Ismail, Modulation of optical, photophysical and electrical properties of poly(3-hexylthiophene) via Gd:CdS nanoparticles, Optik 260 (2022) 169092.

[10] J.W. Chen, X. J.Yin, L.Li, B.Hong, X.Fan, Z.Chen, B.Xue, C.Zhang, H., One-pot synthesis of CdS nanocrystals hybridized with single-layer transition-metal dichalcogenide nanosheets for efficient photocatalytic hydrogen evolution, Angewandte Chemie-International Edition 54(4) (2015) 1210-4.

[11] K.E.Q.-G. Nieto-Zepeda, J. G.Rodríguez-Rosales, K.Guillén-Cervantes, A.Santos-Cruz, J.Zelaya-Ángel, O.de Moure-Flores, F., Optoelectronic properties of Cl and F doped CdS thin films grown by chemical bath deposition, Optik 226(2) (2021) 166004.

ISSN: 2472-3703 DOI: 10.6911/WSRJ.202304_9(4).0029

[12] A.K. Vishwakarma, L. Yadava, Fabrication and characterization of CdS doped ZnO nano thick films, Vacuum 155 (2018) 214-218.

[13] F.T. Munna, P. Chelvanathan, K. Sobayel, K. Nurhafiza, D.K. Sarkar, M. Nour, H. Sindi, M. Rawa, K. Sopian, N. Amin, M. Akhtaruzzaman, Effect of zinc doping on the optoelectronic properties of cadmium sulphide (CdS) thin films deposited by chemical bath deposition by utilising an alternative sulphur precursor, Optik 218 (2020) 165197.

[14] b. Wenlong Zhena, Xiaofeng Ninga, Baojun Yanga, Yuqi Wua,∗, Zhen Lia, Gongxuan Lua, The enhancement of CdS photocatalytic activity for water splitting via anti-photocorrosion by coating Ni2P shell and removing nascent formed oxygen with artificial gill, Applied Catalysis B: Environmental 221 (2018) 243-257.

[15] J.C. Wei, Yawen Zhang, Hongyang Zhuang, Zanyong Yu, Yan, Hierarchically porous S-scheme CdS/UiO-66 photocatalyst for efficient 4-nitroaniline reduction, Chinese Journal of Catalysis 42(1) (2021) 78-86.

[16] W. Zhong, Shijie He, Min Wang, DaWang, ZongpengLin, ZhipingTu, WenguangYu, Jiaguo, The pulsed laser-induced Schottky junction via in-situ forming Cd clusters on CdS surfaces toward efficient visible light-driven photocatalytic hydrogen evolution, Applied Catalysis B: Environmental 258 (2019) 117967.

[17] T. Di, B. Cheng, W. Ho, J. Yu, H. Tang, Hierarchically CdS–Ag2S nanocomposites for efficient photocatalytic H2 production, Applied Surface Science 470 (2019) 196-204.

[18] J. Van Embden, J.O. Mendes, J.J. Jasieniak, A.S.R. Chesman, E. Della Gaspera, Solution-processed CuSbS2 thin films and superstrate solar cells with CdS/In2S3 buffer layers, ACS Applied Energy Materials 3(8) (2020) 7885-7895.

[19] N.K.C. Das, J.Farhad, S. F. U.Sen Gupta, A. K.Ikball Ahamed, E. M. K.Rahman, K. S.Wafi, A.Alkahtani, A. A.Matin, M. A.Amin, N., Effect of substrate temperature on the properties of RF sputtered CdS thin films for solar cell applications, Results in Physics 17 (2020) 103132.

[20] M.G. Nadarajah, K. S. Singh, V. N., Sputtered cadmium sulfide (CdS) buffer layer for kesterite and chalcogenide thin film solar cell (TFSC) applications, Journal of Nanoscience and Nanotechnology 20(6) (2020) 3909-3912.

[21] A. Kumar, R.K. Sharma, N. Goyal, S. Gautam, Synthesis, characterization & study of Ni-doped CdS nanoparticle for high voltage application, Vacuum 160 (2019) 75-80.

[22] N. Nobari, M. Behboudnia, R. Maleki, Systematics in morphological, structural and optoelectrical properties of nanocrystalline CdS thin films grown by electrodeposition method, Materials Science and Engineering B-Advanced Functional Solid-State Materials 224 (2017) 181-189.

[23] S.D. Chander, M. S., Optical and structural constants of CdS thin films grown by electron beam vacuum evaporation for solar cells, Thin Solid Films 638 (2017) 179-188.

[24] J.B. Bora, A.Arandhara, G.Saikia, P. K., Effect of Ag doping on the optical and structural properties of CdS/ polyvinyl alcohol thin films by thermolysis process, Thin Solid Films 734 (2021) 138847.

[25] V. Bilgin, EmrahDemirselcuk, BarbarosErtürk, Kadir, Characterization of CdS films and CdS/Si heterojunctions prepared by ultrasonic spray pyrolysis and their response to light, Physica B: Condensed Matter 599 (2020) 412499.

[26] D. Xiang, L. Yang, Y. Hou, J. Zhu, M. Yang, Hybrid CdS-Au nanochains with enhanced photoelectrochemistry, Vacuum 168 (2019) 108866.

ISSN: 2472-3703 DOI: 10.6911/WSRJ.202304_9(4).0029

[27] M.A. Shkir, I. M.Khan, A.Khan, M. T.El-Toni, A. M.AlFaify, S., A facile spray pyrolysis fabrication of Sm:CdS thin films for high-performance photodetector applications, Sensors and Actuators a-Physical 306 (2020) 111952.

[28] S.Z. Wang, Xiang Bie, Jiaying Gong, HuiPei Cao, Meng Zhang, ShanJiang, YuchengShen, YueWang, Linjun, Influence of Cu doping on physical and photo-electrochemical properties of CdS thin films prepared by RF magnetron sputtering, Materials Science in Semiconductor Processing 133 (2021) 105933.

[29] Y.J. Ma, Peng FeiLi, Yong Song, Yue LiZhou, Feng Qun, A prototypical near-infrared light-emitting diode from CdS/Si heterojunctions based on the defect emissions in the interface, Journal of Luminescence 240 (2021) 118434.

[30] I.R. Chavez-Urbiola, M.I. Pintor-Monroy, F.J. Willars-Rodriguez, Y.V. Vorobiev, R. Ramirez-Bon, M.A. Quevedo-Lopez, Effects of aluminum doping upon properties of cadmium sulfide thin films and its effect on ITO/CdS:Al/NiOx/Ni/Au diodes, Journal of Applied Physics 126(11) (2019) 115702.

[31] I.M.K. Ashraf, Mohd TaukeerHariprasad, K.Valanarasu, S.Alshahrani, T.Almohammedi, AbdullahAlgarni, H.Shkir, MohdAlFaify, S., Enhancement in photodetection properties of Ag/CdS/Ag devices through novel rare-earth metal Tb doping, Materials Letters 285 (2021) 129174.

[32] M. Shkir, Z. R.Alshammari, Abdullah S.Gandouzi, M.Ashraf, I. M.AlFaify, S., A comprehensive experimental investigation of La@CdS nanostructured thin films: Structural, opto-nonlinear and photodetection properties, Surfaces and Interfaces 24 (2021) 101063.

[33] B. Singh, J. Singh, R. Kaur, R.K. Moudgil, S.K. Tripathi, Quantitative measurement of transport properties: Ag-doped nanocrystalline CdS thin films, RSC Advances 7(85) (2017) 53951-53962.

[34] A.A.M. Aboud, AyanRevaprasadu, Neerish Mohamed, Ahmed Nagaty, The effect of Cu-doping on CdS thin films deposited by the spray pyrolysis technique, Journal of Materials Research and Technology 8(2) (2019) 2021-2030.

[35] M.A.S. Manthrammel, MohdShafik, S.Anis, Mohd AlFaify, S., A systematic investigation on physical properties of spray pyrolysis–fabricated CdS thin films for opto-nonlinear applications: An effect of Na doping, Journal of Materials Research 35(4) (2020) 410-421.

[36] X. Xie, R. Wang, Y. Ma, J. Chen, Z. Shi, Q. Cui, Z. Li, C. Xu, Sulfate-functionalized core–shell ZnO/CdS/Ag2S nanorod arrays with dual-charge-transfer channels for enhanced photoelectrochemical performance, ACS Applied Energy Materials 5(5) (2022) 6228–6237.

[37] Y. Zhang, Z. Zhang, W. Yao, X. Liang, Microstructure, mechanical properties and corrosion resistance of high-level hard Nb-Ta-W and Nb-Ta-W-Hf multi-principal element alloy thin films, Journal of Alloys and Compounds 920 (2022) 166000.

[38] Y. Gong, S.T. Misture, P. Gao, N.P. Mellott, Surface roughness measurements using power spectrum density analysis with enhanced spatial correlation length, The Journal of Physical Chemistry C 120(39) (2016) 22358-22364.

[39] Y. Zhang, Z. Jin, D. Liu, Z. Tan, B.B. Mamba, A.T. Kuvarega, J. Gui, S-scheme Bi2S3/CdS nanorod heterojunction photocatalysts with improved carrier separation and redox capacity for pollutant removal, ACS Applied Nano Materials 5(4) (2022) 5448-5458.

[40] M.R.A. Mohammad, Duha S.Mohammed, Mustafa K. A., Synthesis of Ag-doped TiO2 nanoparticles coated with carbon nanotubes by the sol–gel method and their antibacterial activities, Journal of Sol-Gel Science and Technology 90(3) (2019) 498-509.

ISSN: 2472-3703 DOI: 10.6911/WSRJ.202304_9(4).0029

[41] M.K.A.A. Mohammed, Duha S.Mohammad, Mohammad R., Studying antimicrobial activity of carbon nanotubes decorated with metal-doped ZnO hybrid materials, Materials Research Express 6(5) (2019) 055404.

[42] M.K.A.A.-M. Mohammed, Ali K.Khalaf, Haider A., Deposition of multi-layer graphene (MLG) film on glass slide by flame synthesis technique, Optik 127(20) (2016) 9848-9852.

[43] J. Bora, A. Borthakur, G. Arandhara, P.K. Saikia, Effect of Ag doping on the optical and structural properties of CdS/polyvinyl alcohol thin films by thermolysis process, Thin Solid Films 734 (2021) 138847.

[44] D. Xiang, X. Hao, Z. Jin, Cu/CdS/MnOx nanostructure-based photocatalyst for photocatalytic hydrogen evolution, ACS Applied Nano Materials 4(12) (2021) 13848-13860.

[45] A.A.A. Ahmed, N.M. Al-Hesni, A.H. Al-Osta, M.L. Al-Salmi, K.A. Manssor, S.M. Ja'adan, B.A. Al-Asbahi, S.M.H. Qaid, H.M. Ghaithan, W.A. Farooq, Influence of single and dual doping (Ag and Co) on the optical properties of CdS quantum dot thin films for solar application, Optik 246 (2021) 167824.

[46] F.-K. Shang, M.-Y. Qi, C.-L. Tan, Z.-R. Tang, Y.-J. Xu, Nanoscale assembly of CdS/BiVO4 hybrids for coupling selective fine chemical synthesis and hydrogen production under visible light, ACS Physical Chemistry Au 2(3) (2022) 216–224.